ADVANCED OPTICAL MATERIALS
www.advopticalmat.de

Tunable Microlasers Modulated by Intracavity Spherical Confinement with Chiral Liquid Crystal

*Yifan Zhang, Zhiyi Yuan, Zhen Qiao, Devesh Barshilia, Wenjie Wang, Guo-En Chang, and Yu-Cheng Chen**

Manipulation of laser emission offers promising opportunities for the generation of new spatial dimensions and applications, particularly in nanophotonics, super-resolution imaging, and data transfer devices. However, the ability to control laser modes and wavelength in a microcavity remains challenging. Here, a novel approach is demonstrated to control laser modes by manipulating the 3D-optical confinement, chirality, and orientations in a Fabry–Pérot microcavity with cholesteric liquid crystal droplets. Different configurations of intracavity micro-/nanostructures generate versatile dimensions of laser modes, while the significantly reduced laser mode volume further leads to single-mode lasing. Theoretical analysis is carried out to support this interesting discovery. Finally, switchable lasing wavelength with various surface anchoring forces and pH interactions is demonstrated. This novel concept not only provides a simple yet highly versatile method to manipulate laser emissions, but deepens insight into how molecules interact with and modulate laser light, laying the foundation for the development of tunable photonic devices at the molecular level. Promising applications include highly selective laser devices, laser-emission imaging, and bioinspired sensing.

Manipulation of laser emission has led to ground-breaking applications in optomechanics,[1–3] super-resolution imaging,[4,5] and tunable optical devices in the past decade.[6,7] Numerous methods have been developed by placing engineered elements inside or outside a Fabry–Pérot (FP) cavity to control the optical properties of laser emission.[8–13] Most studies focused on either the tunability of laser modes or switching of lasing wavelengths. However, the capability to control both lasing spectra and laser modes in a microresonator remains challenging due to the lack of efficient mechanisms to overcome mode competitions. Conventional FP cavity relies on two highly reflected planar mirrors to form a resonator, in which whole-body interactions between the electromagnetic field and the gain medium can be utilized for intracavity detection and manipulation.[14–18] The structure of within the FP cavity can also alter the lasing output characteristics sensitively (e.g., laser mode, threshold, and lasing spectrum). Herein, we developed a tunable laser by configuring the optical confinement, chirality, and polarization at the nanoscale with liquid crystals (LCs) in FP microcavity.

LCs have received emerging attention owing to its tunability, in which the orientation of the elongated LC molecules will change under an external stimulus. Additionally, anisotropic optical characteristics can be manipulated dynamically by changing the internal structures in cholesteric LC (CLC). Based on the unique features, LCs have been extensively used in biosensing, temperature detection, and whispering-gallery mode (WGM) laser resonators.[19–24] As the chiral dopant increases in CLC droplets, the number of periodic refractive index variation (periodic shells) increases to form higher structural confinement and chirality. Recent studies have further applied CLC microdroplets to obtain spherical or lateral confinement of optical modes.[25–27]

In this work, we explored the lasing properties of a hybrid FP cavity by modulating light confinement and interactions in a FP resonator. Different configurations of micro-/nanostructured CLC–WGM droplet allowed the versatile design of optical confinement, chirality, and molecular orientation. Taking advantage of the vast complexity and tunability of CLCs, this novel concept provides a simple yet highly versatile method to manipulate laser modes and lasing wavelengths. Three representative CLC structures were prepared and analyzed in this work, with the pitch length (p_o) designed to be larger ($p_o >> \lambda$), close to ($p_o \sim \lambda$), and smaller ($p_o < \lambda$) than the lasing wavelength (λ). **Figure 1**a shows that as the pitch length becomes smaller,

Dr. Y. Zhang, Z. Yuan, Dr. Z. Qiao, Prof. Y.-C. Chen
School of Electrical and Electronics Engineering
Nanyang Technological Universit
50 Nanyang Ave, Singapore 639798, Singapore
E-mail: yucchen@ntu.edu.sg
D. Barshilia, Prof. G.-E. Chang
Department of Mechanical Engineering
National Chung Cheng University
Minhsiung, Chiayi 62102, Taiwan, ROC
Prof. W. Wang
Key Lab of Advanced Transducers and Intelligent Control System
of Ministry of Education
Taiyuan University of Technology
Taiyuan 030024, P. R. China
Prof. Y.-C. Chen
School of Chemical and Biomedical Engineering
Nanyang Technological University
62 Nanyang Drive, Singapore
The ORCID identification number(s) for the author(s) of this article can be found under https://doi.org/10.1002/adom.201902184.

DOI: 10.1002/adom.201902184

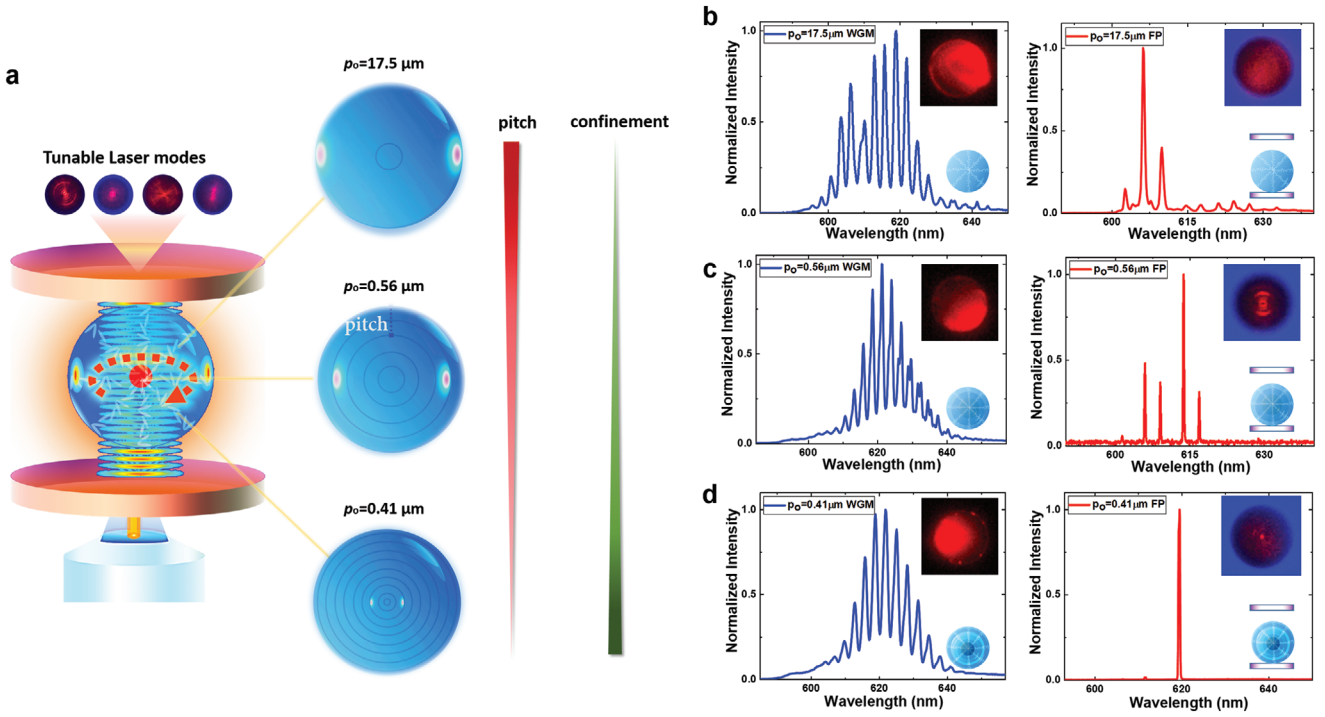

Figure 1. a) Schematic diagram of the hybrid Fabry–Pérot (FP) cavity. With decrease of pitch length, light is confined toward the droplet center to form resonance inside the FP cavity. The three spheres do not represent actual simulation results. b–d) Comparison of lasing spectra between whispering-gallery mode (WGM) and hybrid WGM–FP cavity with increasing chirality. b) Droplets with p_o = 17.5 μm. c) Droplets with p_o = 0.56 μm. d) Droplets with p_o = 0.41 μm. The left panels show WGM lasing while the right panels show WGM droplet confined in FP cavity. Inserts show bright field images of each laser modes. (Droplet diameter = 25 μm throughout the article unless specified otherwise.)

light can be highly focused inside different equatorial planes of the CLC droplets. We further discovered that as the nano-confinement increases, single-mode lasing becomes possible. Laser mode volume was also significantly reduced with high CLC concentric spherical confinement. Theoretical and experimental analysis of resonances were carried out to support these interesting phenomena. Finally, we showed how the molecular interaction alters the symmetric confinement on CLC microcavity and strongly affects the output lasing wavelength. pH-responsive lasing was also conducted to exploit the potential for tuning lasers with intracavity biochemical reactions. By controlling the chirality, droplet–cavity length, pitch size, anchoring forces, or molecular interactions, lasing emissions (laser mode and spectral wavelength) can by fully programmed. We envision this work may bring a significant impact on programmable laser devices, super-resolution laser imaging, and bioinspired photonic applications.

We first investigated the effect of pitch lengths toward lasing spectrum, including p_o = 17.5, 7, 3.50, 2.33, 1.75, 0.88, 0.56, and 0.41 μm separately. However, we found that the lasing behaviors were very similar in droplets with pitch length larger than lasing wavelength (Figure S1, Supporting Information). Multipeaks following WGM was found in all cases. Therefore, we selected three representative pitch lengths for further investigation, which represent larger ($p_o >> \lambda$), close to ($p_o \sim \lambda$), and smaller ($p_o < \lambda$) than the lasing wavelength (λ). Figure 1a depicts the three major CLC structures used in this work by increasing the chiral dopant concentrations to form pitch length (p_o) of 17.5, 0.56, and 0.41 μm, respectively. First, we explore the interactions when a WGM laser is placed inside a FP cavity, herein three configurations were designed in the first part of the experiment. Here in this section, we discuss the effect of pitches by using lasing spectrum, laser mode, lasing thresholds, and lasing intensity.

As shown in Figure 1b–d, the left panel shows pure WGM laser whereby the right panel shows the laser emission encapsulated in a FP cavity. As the chiral dopant concentration increases, the pitch lengths decrease while the number of periodic shells increases, thus improving the spherical confinement of light. Surprisingly, we found unusual and distinctive lasing spectra as we change the spherical confinement in a fixed FP cavity. As shown in Figure 1b, for p_o = 17.5 μm, the lasing spectrum in FP remains similar to pure WGM laser; however, the bandwidth (FWHM) is significantly reduced. When p_o decreases to 0.56 μm, the bandwidth becomes significantly narrower (Figure 1c). A sharp lasing ring is visible inside the droplet. When further shrinking p_o to 0.41 μm, we surprisingly obtained single-mode lasing with a single bright red dot in the droplet center (Figure 1c,d insert).

Besides lasing spectra and laser mode profile, differences were also clearly observed in lasing thresholds and intensity. **Figure 2**a–c presents the lasing threshold for the three droplets. For p_o = 17.5 μm, droplets in both cavities have the same threshold value, which is about 58.7 μJ mm^{-2}. As the pitch size p_o becomes smaller (0.58 and 0.41 μm), the lasing threshold significantly decreased 3–4 times lower than that of the pure

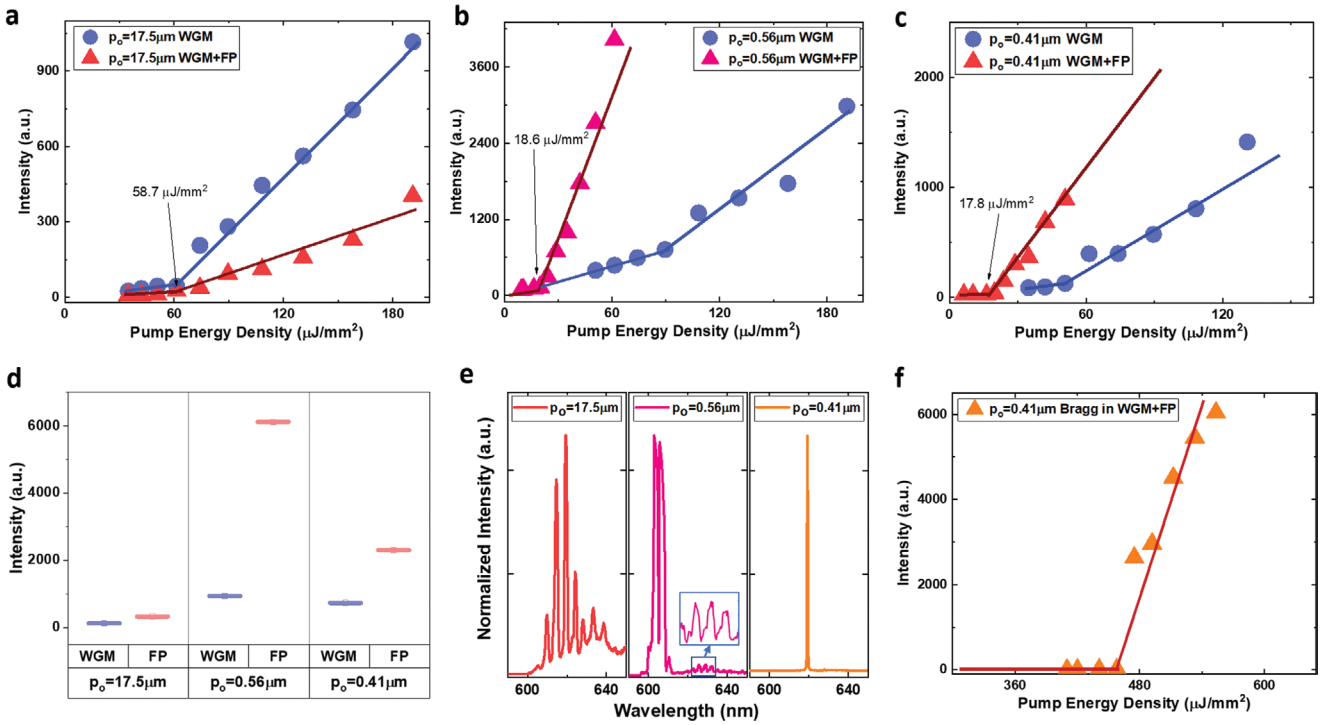

Figure 2. a–c) Threshold behaviors for droplets with p_o = 17.5, 0.56, and 0.41 μm. d) Lasing intensity for the three droplets under low pump energy density (100 μJ mm^{-2}). e) Lasing spectra for the three droplets at very high pump energy density. f) Spectrally integrated laser output as a function of the pump energy density for droplet with p_o = 0.41 μm. Single-mode lasing appears when pump power increased to 450 μJ mm^{-2}. (Droplet diameter = 25 μm throughout the article unless specified otherwise.)

WGM cavity. However, only a slight difference was found between 0.58 and 0.41 μm. Next in Figure 2d, we compared the lasing intensity of the three droplets under a relative "low" pump energy density (fixed at 100 μJ mm^{-2}). As seen in Figure 2d, p_o = 17.5 μm presented the lowest lasing intensity while p_o = 0.56 μm presented the strongest intensity. However, p_o = 0.41 μm showed a relative lower intensity likely due to the transition between multimode to single-mode lasing in Bragg region. Note that in all three cases, droplets in FP presented a higher lasing intensity than pure WGM. In Figure 2e, we further compared the lasing spectra under a high pump intensity (500 μJ mm^{-2}). No difference was seen for p_o = 17.5 μm. While two lasing bands were found in p_o = 0.56 μm, this indicates a competition or transition of laser mode emerging. In p_o = 0.41 μm, a sharp and high-intensity single-mode lasing appears, which marks significant characteristic of high chirality CLC droplets (Figure 2e). The threshold for single-mode lasing is 450 μJ mm^{-2} (Figure 2f).

The variations of two configurations are further reviewed through free spectral range (FSR) in **Figure 3**a–c. In WGM cavity, all FSRs are linearly proportionate to the inverse of droplet diameter (Figure S2a, Supporting Information). However, the measured FSRs in the FP cavity are incredibly chaotic. The calculated FSRs based on pure FP and WGM cavity are plotted in the same graph for comparison (Figure 3c). The two fitted lines show the theoretical FSR when considering the CLCs in the FP cavity are either conventional FP or WGM resonator. The symbols represent the experimental FSRs measured from randomly selected CLC droplets in FP with different pitch lengths and droplet diameters. The intersection corresponds to the droplet size of 25 μm, where the conditions both fulfill WGM and FP (Figure 3c). It is noteworthy that at very large p_o, the FSR shows the lasing peaks with WGM features (less spherical confinements). As p_o decreases (higher spherical confinement), the data points deviate more from the fitted lines, forming a unique optical pathway, unlike conventional FP cavity. For demonstration, we selected two droplets with the exact diameter but different p_o, which exhibits distinct FSR (Figure S2d,e, Supporting Information) and two droplets with a different diameter, which have the same FSR (Figure S2b,c, Supporting Information).

In order to elucidate the fundamental mechanism, optical simulations have been carried out. The periodic helical twisting, which induces concentric microstructure, is regarded as alternate high (RI = 1.56, $n_{e,5CB}$) and low (RI = 1.50, $n_{o,5CB}$) refractive index distribution inside the sphere (periodic shell). p_o can be calculated by $p_o = \frac{1}{[c]\cdot HTP}$ where the helical twisting power (HTP) is 7.14 μm^{-1} for chiral dopant CB15.[28] Here in Figure 3d–f, we present the simulation of the three CLC droplets as pure WGM cavity. No significant differences were noted as p_o become smaller. However, the number of higher-order modes increased as p_o decreases, which also influences the resonance frequency. Resonance could form inside the droplets among those rings, like the schematic in Figure 1a. Moreover, owing to the larger refractive index difference between the CLC and solvent, resonance is more prone to form near the boundary than interdroplet rings in the WGM cavity, which is

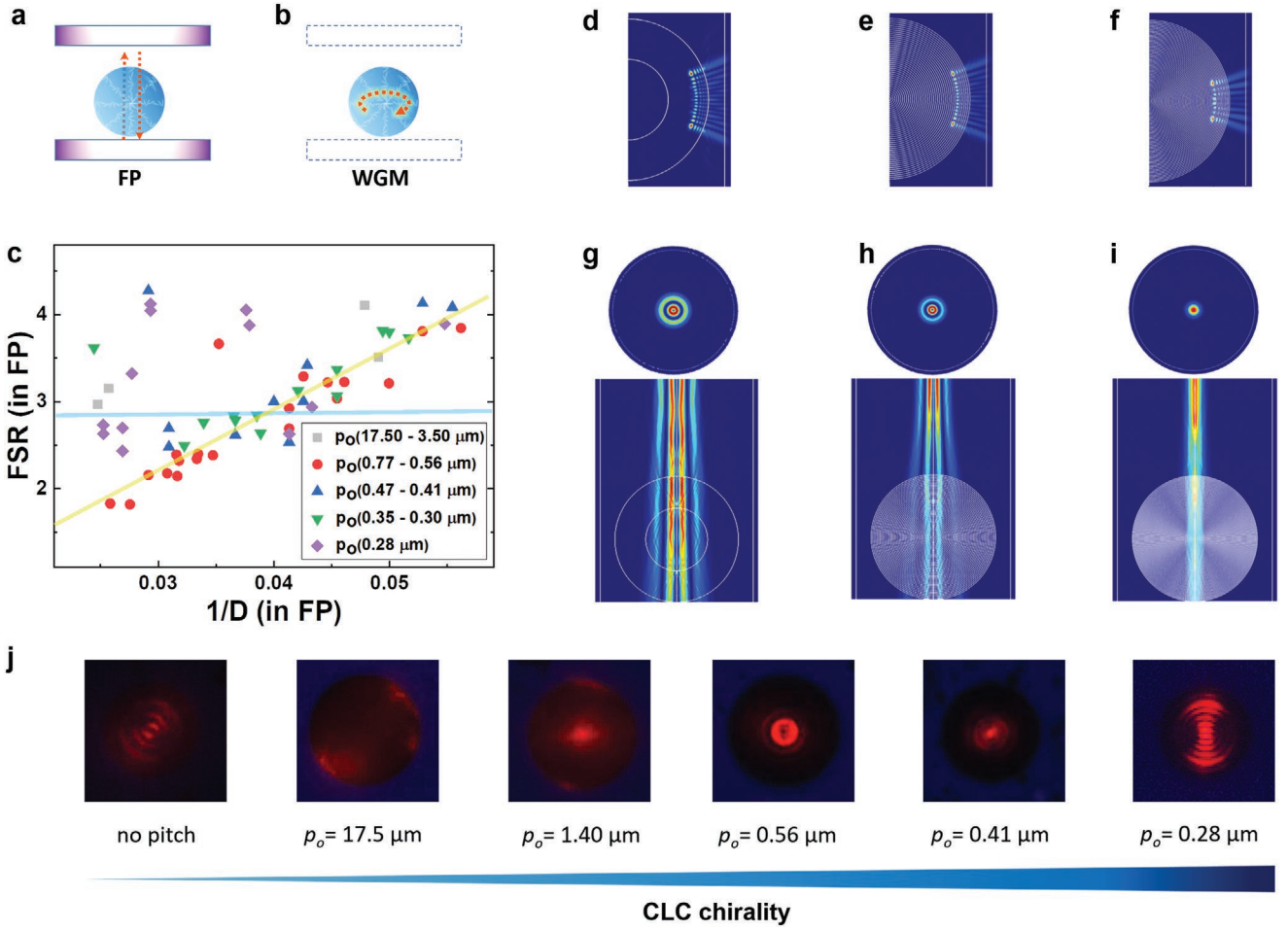

Figure 3. a,b) Schematic diagram of light path in Fabry–Pérot (FP) cavity and whispering-gallery mode (WGM) resonator. c) Free spectral range (FSR) in the hybrid cavity. The FSRs are no longer following the relationship in pure FP cavity. The yellow linearly fitted lines are calculated FSR values in WGM. The light blue linearly fitted lines are calculated FSR values in FP cavity. d–i) Simulation results of cholesteric liquid crystal (CLC) droplet with pitch of 17.5, 0.56, and 0.41 μm. d–f) CLC droplets in pure WGM cavity. g–i) CLC droplets in hybrid WGM–FP cavity. The top row shows that mode distribution viewed from the top, while the bottom row shows the cross-section from side view. The mirror spacing was set to be 40 μm where the CLC droplet set to be 25 μm is assumed to the center. j) Laser modes modulation by increasing the chirality in CLC droplets. No pitch = nematic liquid crystal droplet (without chiral dopant). Distinctive mode is confined in the droplet center.

supported by the FSR analysis (Figure S2, Supporting Information). Next, we modeled the case when the WGM droplet is sandwiched between two DBR mirrors. In order to match with the experimental setup, the simulation model introduced a space before the top mirror. The simulation results show that the FP cavity made a significant impact on the WGM modes and changed the mode profiles significantly (Figure 3g–i). The high refractive index of the droplet boundary confined the reflected light toward the droplet center. The simulation reveals that the incorporation of FP mirrors helps to confine and reduces the mode volume, which explains why the intracavity thresholds are much lower than in WGM cavity.

The consequence is apparent that the high refractive index of the droplet boundary confined the reflected light toward the droplet center (Figure S3, Supporting Information). With the existence of mirrors, the droplet provides better light confinement in the core region. The effective *Q*-factor was also significantly increased to 3×10^5. Resonance can form in any layer of the high–low refractive index rings, depending on the actual refractive index difference and molecule orientation inside the helical structure. The simulation reveals that more periodic shells have higher chances to form resonance toward the tiny cavity center, facilitating single-mode lasing. In order to demonstrate manipulation of laser mode profile over p_o changes, a series of modes were taken by increasing the intracavity chirality (Figure 3j).[29] When no chiral dopant is induced, no pitch will be formed within the droplet. The nematic LC droplet is therefore comparable to the mode in glass bead in a FP cavity. As chirality increases, the introduction of chirality induces LCs to twist and this the p_o decreases. As one can see, distinct laser modes appear under different CLC chirality. When the pitch size (p_o) becomes closer to lasing wavelength, resonance starts to develop inside the droplet. The spherical light confinement in the droplet center becomes clear when p_o is close to lasing wavelength owing to the Bragg reflection from CLC.

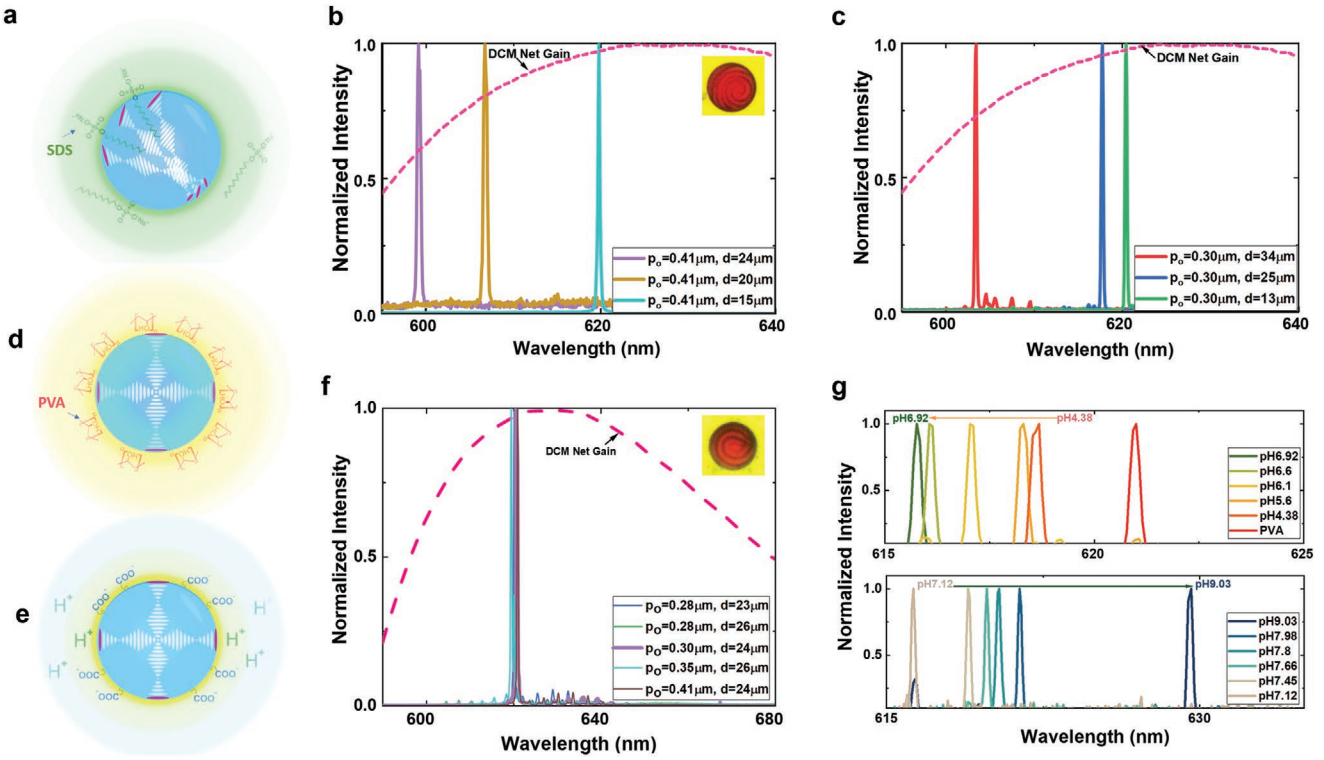

Figure 4. a) Lasing droplets in sodium dodecyl sulfate (SDS). SDS promotes homeotropic anchoring of liquid crystals (LCs). Single-mode lasing wavelength shifts in different chirality and sizes. b,c) Droplets with same chirality, it appears blue shift with increasing of sizes. d) Lasing droplets in polyvinyl alcohol (PVA). e) Schematic of pH sensing with droplets in PVA. f) PVA provides tangential anchoring of LCs, single-mode lasing occurs near 620 nm regardless of the droplets size and chirality. g) Single-mode lasing wavelength experiences shifting in different pH. Lasing spectra exhibit blue shift with increase of pH in acidic buffer solution (from pH 4.38 to pH 6.92), whereas it appears red shift in base buffer solution (from pH 7.12 to pH 9.03). Droplet size = 25 μm for all experiments.

Lasing in the hybrid cavity is strongly influenced by the droplet internal geometry, while the geometry of droplets dramatically depends on its chirality and surface anchoring forces. There are two types of anchoring forces, tangential and homeotropic anchoring. In tangential anchoring, the droplet shows stable concentric fingerprint rings with different pitches. In homeotropic anchoring, the arrangement is more complicated. While the surfactant is trying to align the LC molecule perpendicular to the surface, the chiral dopant is twisting them into a helix. The competition between the anchoring force and the helical twisting force causes twisting layer deformation inside the droplet. As a result, instead of isotropic chiral, the droplets are in spherulite-like structures under the microscope. The concentric rings arranged in conical shape are visualized.[30]

In order to investigate how surface anchoring may affect lasing wavelength, CLC droplets were dispersed in two different solutions, polyvinyl alcohol (PVA) and sodium dodecyl sulfate (SDS). The representative structures are plotted in **Figure 4**a–d respectively. In SDS, the wavelength varies dramatically, owing to the frustration of droplet geometry. Based on the same droplet size but with different chirality (pitch), as seen in Figure 4b,c, the lasing wavelength is 599.40 and 618.00 nm for p_o = 0.41 and 0.30 μm, respectively. For droplets with the same chirality but different sizes, the lasing wavelength blue shifts with an increase of diameter (d). The single-mode lasing wavelength blue shifts from 620.00 to 599.40 nm for d = 15 to 24 μm in p_o = 0.41 μm. Correspondingly, when d increases from 13 to 34 μm in p_o = 0.30 μm, the wavelength blue shifts from 620.40 to 603.30 nm. In contrast, PVA promotes tangential anchoring, whereas SDS promotes homeotropic anchoring. Droplet structure with tangential anchoring is more stable than homeotropic anchoring (Figure 4d), as well as the lasing wavelength. Droplets display consistent onion ring structures throughout the three p_o. As presented in Figure 4f, the single-mode lasing wavelength in PVA remains around 620.50 nm regardless of its chirality and sizes.

Surface anchoring forces are the result of the electrostatic force exerted by external molecules (surfactant) on a LC microsphere surface. Nevertheless, the selectivity of molecules is essential for biochemical sensing, which means only the presence of interested analytes can trigger the droplet internal structure changes. In order to testify this intracavity resonator's ability in selective molecular sensing, a pH-sensitive dopant (4'-*n*-hexylbiphenyl-4-carboxylic acid) was chosen to incorporate in the droplets. The doped CLC droplets were immersed in a solution with a range of pH values (Figure 4e). The long hydrocarbon chain of the dopant can lead to bulk changes of LC orientation after protonation–deprotonation, which in turn influences the lasing activities. The lasing peaks are 618.68, 618.31, 617.03, 616.06, and 615.76 nm, respectively, for pH 4.38, 5.6, 6.1, 6.6, and 6.92 (Figure 4g). There is a significant blue shift with an increase in pH value. However, when pH reaches

to 7.12, the lasing peak starts to red shift to 616.28 nm. Further red shifting to 618.90, 619.80, 620.40, 621.37, and 629.60 nm was detected for pH 7.45, 7.66, 7.8, 7.98, and 9.03, respectively (Figure 4g). This phenomenon agrees on the critical value (pH 7.0) with past studies. In this experiment, a total blue shift of 2.92 nm, and a red shift of 13.31 nm was measured. The results indicate that intracavity FP lasing is not only affected by surface anchoring forces but also extremely sensitive to biochemical reactions within the resonator. Moreover, selectivity can be activated by selecting a suitable dopant.

In this research, we proposed a novel approach to manipulate laser modes in a FP microcavity with CLC droplets. Both experimental and theoretical studies have revealed how the intracavity structure dramatically change the laser output. Unlike conventional FP cavity which usually confines the light in the vertical direction, the addition of CLC droplet provided an 3D-confined optical resonance in the FP cavity to achieve modes with higher spatial and spectral resolution. Our results show that hybrid WGM–FP cavity can generate and control higher order laser modes with an improved Q-factor. Higher chirality droplets also help support ring resonance close to the center and reduce the laser mode volume significantly. Single-mode lasing can be easily realized in such a hybrid cavity when the pitch length is near the laser emission wavelength, featuring a narrow and strong signal. Besides changing the chirality structure within the droplets, we demonstrated that molecule interactions play an essential role in laser modes. Finally, switchable lasing was demonstrated through localized pH changes due to internal chiral structure variation.

The significance of this research implies that the FP cavity is susceptible to its internal geometric structure, where higher-order lasing modes could be fully manipulated by structural confinement or chirality at the nanoscale. Herein, we would like to point out three promising directions. First, by carefully designing the inner structure, this could be integrated with single-mode on-chip light sources. Different wavelengths and laser modes could be controlled depending on various applications, such as communication and optoelectronics. Second, the sensitivity of this system is expected to be extremely high, owing to its high-quality factor. As such, this system may be very promising for single-molecule applications to achieve extreme high refractive index (RIU) sensing. Lastly, different sensing probes could be incorporated inside the CLC droplet to perform specific biochemical or biophysical sensing.

Experimental Section

Sample Preparation: All chemicals were purchased from Sigma–Aldrich unless specified. The mixture of nematic LC (4′-pentyl-4-biphenylcarbonitrile, 5CB, Tokyo Chemicals), 0.1 wt% laser dye (4-dicyanomethylene-2-methyl-(6-4-dimethylaminostry-1)-4H-pyan, DCM) and chiral dopant (4-cyano-4'-(2-methylbutyl)biphenyl, CB15) was immersed in an ultrasonic bath for 15 min to form a homogenous CLCs. There were eight chiral dopant concentrations, namely 0.8, 2, 4, 6, 8, 16, 25, and 34 wt%. An amount of 1 wt% surfactant, PVA or SDS, was added in DI water to promote desired surface anchoring in the formation of CLC droplets by solvent-induced phase separation (SIPS) method. The CLC mixture was added in the surfactant solution at 1:9 ratio. A vortex mixer shook the final solution for 10 minu. The obtained droplet sizes varied from 7 to 70 µm. To have a fair comparison, 25 µm was selected throughout the whole experimental observations. In the final part of the experiments, 0.1 wt% of pH dopant (4′-*n*-hexylbiphenyl-4-carboxylic acid, Regent Chemicals) was added into the CLC mixture for pH sensing. Different ratios of potassium phosphate monobasic and potassium phosphate dibasic were mixed to get pH buffer solutions ranged from pH 4.38 to 9.03.

Optical Measurements and Setup: The bright field polarized images were taken with a Nikon-E200 Polarized Microscope. The bright field images of the laser emissions were captured by using a CCD (Thorlabs #DCU223C) integrated directly on top of the objective. For the pumping of the CLC microdroplet and the collection of light, an inverted microscopic system (Nikon Ti2) with 20×, NA 0.4 objective was used. Pumping was achieved using an optical parametric oscillator with 5 ns pulse duration (EKSPLA PS8001DR), tuned to 470 nm for DCM dyes. The beam was focused on the microdroplet center. Its diameter at the objective focal plane was ≈16 µm wide. The pump energy density was adjusted by a continuously variable neutral density filter, normally in the range of 0.2– 500 µJ mm^{-2}. The emission light was collected through the same objective then separated by a beam splitter and sent into a charge-coupled device camera and imaging spectrometer (Andor Kymera 328i and Newton 970 EMCCD).

FP Microcavities: The FP microcavity was formed by two customized dielectric mirrors. The bottom mirror (made by Qingdao Novel Beam Technology Co. Ltd, China) has a high reflectivity above 550 nm to provide optical feedback and high transmission around 450 nm for the pump light to pass through, whereas the top mirror (made by Evaporated Coating INC, USA) has a slightly wider reflection band up to 650 nm. Spacers of silica beads were used to ensure the cavity length of 45 µm. The *Q*-factor for the original FP cavity was on the order of 10^3.

Finite-Element Simulations: The optical cavities were simulated using the COMSOL Multiphysics finite element method. The field distribution of the cavity modes is analyzed using eigenfrequency study under axisymmetric conditions. Perfect-matching layers (PMLs) are applied to the outer domains.

Supporting Information

Supporting Information is available from the Wiley Online Library or from the author.

Acknowledgements

The authors would like to thank the Centre of Bio-Devices and Signal Analysis for the lab support andand Nanyang Technological University, Singapore for the internal grant (NAP-SUG M4082308.404).

Conflict of Interest

The authors declare no conflict of interest.

Keywords

cholesteric liquid crystals, high-order laser mode, intracavity interactions, spherical confinement, tunable lasing

Received: December 27, 2019
Revised: March 10, 2020
Published online:

[1] M. Padgett, R. Bowman, *Nat. Photonics* **2011**, *5*, 343.
[2] D. G. Grier, *Nature* **2003**, *424*, 810.
[3] B. K. Singh, H. Nagar, Y. Roichman, A. Arie, *Light: Sci. Appl.* **2017**, *6*, e17050.

[4] G. Vicidomini, P. Bianchini, A. Diaspro, *Nat. Methods* **2018**, *15*, 173.
[5] A. Small, S. Stahlheber, *Nat. Methods* **2014**, *11*, 267.
[6] Z. J. Wong, Y. L. Xu, J. Kim, K. O'Brien, Y. Wang, L. Feng, X. Zhang, *Nat. Photonics* **2016**, *10*, 796.
[7] E. Maguid, R. Chriki, M. Yannai, V. Kleiner, E. Hasman, A. A. Friesem, N. Davidson, *ACS Photonics* **2018**, *5*, 1817.
[8] R. Chriki, E. Maguid, C. Tradonsky, V. Kleiner, A. A. Friesem, N. Davidson, E. Hasman, *Opt. Express* **2018**, *26*, 905.
[9] M. D. Baaske, F. Vollmer, *Nat. Photonics* **2016**, *10*, 733.
[10] D. Naidoo, F. S. Roux, A. Dudley, I. Litvin, B. Piccirillo, L. Marrucci, A. Forbes, *Nat. Photonics* **2016**, *10*, 327.
[11] Z. Qiao, G. Q. Xie, Y. Wu, P. Yuan, J. Ma, L. Qian, D. Fan, *Laser Photonics Rev.* **2018**, *12*, 1800019.
[12] U. D. Zeitner, F. Wyrowski, H. Zellmer, *IEEE J. Quantum Electron.* **2000**, *36*, 1105.
[13] J. Wynne, *IEEE J. Quantum Electron.* **1974**, *10*, 125.
[14] Y. C. Chen, X. Fan, *Adv. Opt. Mater.* **2019**, *7*, 1900377.
[15] Y. C. Chen, X. Tan, Q. Sun, Q. Chen, W. Wang, X. Fan, *Nat. Biomed. Eng.* **2017**, *1*, 724.
[16] X. Wu, M. K. K. Oo, K. Reddy, Q. Chen, Y. Sun, X. Fan, *Nat. Commun.* **2014**, *5*, 3779.
[17] Z. Yuan, Z. Wang, P. Guan, X. Wu, Y. C. Chen, *Adv. Opt. Mater.* **2020**, *8*, 1901596.
[18] M. C. Gather, S. H. Yun, *Nat. Photonics* **2011**, *5*, 406.
[19] G. Pirnat, M. Humar, I. Muševič, *Opt. Express* **2018**, *26*, 22615.
[20] S. S. Lee, J. B. Kim, Y. H. Kim, S. H. Kim, *Sci. Adv.* **2018**, *4*, eaat8276.
[21] M. Humar, *Liq. Cryst.* **2016**, *43*, 1937.
[22] L. Zhao, Y. Wang, Y. Yuan, Y. Liu, S. Liu, W. Sun, J. Yang, H. Li, *Opt. Commun.* **2017**, *402*, 181.
[23] M. Humar, M. Ravnik, S. Pajk, I. Muševič, *Nat. Photonics* **2009**, *3*, 595.
[24] D. S. Kim, W. Lee, T. Lopez-Leon, D. K. Yoon, *Small* **2019**, *15*, 1903818.
[25] X. Wu, Y. Wang, Q. Chen, Y. C. Chen, X. Li, L. Tong, X. Fan, *Photonics Res.* **2019**, *7*, 50.
[26] Y. Li, N. Khuu, E. Prince, M. Alizadehgiashi, E. Galati, O. D. Lavrentovich, E. Kumacheva, *Sci. Adv.* **2019**, *5*, eaav1035.
[27] Y. Li, J. J.-Y. Suen, E. Prince, E. M. Larin, A. Klinkova, H. Therien-Aubin, S. Zhu, B. Yang, A. S. Helmy, O. D. Lavrentovich, E. Kumacheva, *Nat. Commun.* **2016**, *7*, 12520.
[28] S. W. Ko, S. H. Huang, A. Y.-G. Fuh, T. H. Lin, *Opt. Express* **2009**, *17*, 15926.
[29] M. N. Krakhalev, V. Y. Rudyak, O. O. Prishchepa, A. P. Gardymova, A. V. Emelyanenko, J. H. Liu, V. Y. Zyryanov, *Soft Matter* **2019**, *15*, 5554.
[30] G. Cipparrone, A. Mazzulla, A. Pane, R. J. Hernandez, R. Bartolino, *Adv. Mater.* **2011**, *23*, 5773.

